

IFUP-TH 23/95

Scaling and topology in the 2-d $O(3)$ σ -model on the lattice with the fixed point action¹

(Revised version)

Federico Farchioni, Massimo D'Elia
Dipartimento di Fisica dell'Università and I.N.F.N.
Piazza Torricelli 2, I-56126 Pisa, Italy.

Alessandro Papa²
Institute for Theoretical Physics
University of Bern
Sidlerstrasse 5, CH-3012 Bern, Switzerland

November 2017

Abstract

We study scaling properties and topological aspects of the 2-d $O(3)$ non-linear σ -model on the lattice with the parametrized fixed point action recently proposed by P. Hasenfratz and F. Niedermayer. The behavior of the mass gap confirms the good properties of scaling of the fixed point action. Concerning the topology, lattice classical solutions are proved to be very stable under local minimization of the action; this outcome ensures the reliability of the cooling method for the computation of the topological susceptibility, which indeed reproduces the results of the field theoretical approach. Disagreement is instead observed with a different approach in which the fixed point topological charge operator is used: we argue that the discrepancy is related to the ultraviolet dominated nature of the model.

¹Work supported in part by Fondazione "A. Della Riccia" (Italy).

²On leave from the Department of Physics, University of Pisa and I.N.F.N., Pisa.

1 Introduction

Simulating a theory on the lattice is the most (and often the only) reliable mean to get an insight into its non-perturbative aspects. Once the theory has been put on the lattice, the non-trivial question is how to correctly reach the continuum limit. The standard procedure of adjusting the bare parameters of the lattice theory closer and closer to the critical values (where the lattice theory is expected to reproduce the continuum) is plagued by critical slowing-down and finite-size effects: in practice one is forced to simulate the theory at finite cut-off, where the systematic effects of discretization, heavily coming into play, can be removed only by an – often ambiguous – extrapolation. A way to reduce lattice artifacts is to use perturbatively improved lattice actions [1], whose performance in numerical simulation is not, however, under theoretical control.

A radical solution to the problem [2] is to use perfect actions, i.e. lattice actions whose spectrum is completely free of lattice artifacts. Wilson’s renormalization group theory [3] ensures that the fixed point (FP) of a renormalization group (RG) transformation and all lattice actions of the renormalized trajectory (RT) – which is the asymptotic flux line under repeated RG transformations – are perfect (quantum) actions in the above mentioned sense. The FP action, in particular, represents the classical perfect action, having the same classical properties of the continuum theory [2].

A method for the determination of the FP of asymptotically free theories has been proposed in a recent paper [2]. The procedure has been applied to the 2-d $O(3)$ non-linear σ -model on the lattice, and a parametrization of the FP action A_{FP} suitable for numerical simulations has been found. Strong numerical evidences [2] indicate that the action A_{FP} is a good approximation of the perfect action at small correlation lengths also. This agrees with the general remark by Wilson [4] that the FP action is (quantum) perfect at 1-loop order in perturbation theory. A formal argument for this statement is presented in [5] and a further support comes from a specific 1-loop calculation in the $O(3)$ σ -model [6].

In the first part of this paper, we test the scaling properties of the FP action of Ref. [2] up to very small correlation lengths: we study the physical scaling of the mass gap – which is the only relevant spectral property in the $O(3)$ σ -model – by comparing different lattice definitions; we also check the rotation invariance.

The second part of this work is devoted to the study of the topological properties of the model with the FP action: in particular, we address ourselves to the problem of extraction from the lattice of the topological susceptibility of the $O(3)$ σ -model [7][8][9][10][11][12][13][14]. We present different approaches to the subject – the field theoretical [15], the geometrical [7] and the cooling [9][16] methods – and compare their outcomes. In this respect, we argue that the cooling method can be

safely applied with the FP action, since it possesses scale invariant classical solutions [2] and no loss of topological signal is expected during the procedure of minimization. The scaling of topological susceptibility is a rather involved matter since the semiclassical approximation [17][18] and some numerical evidences [19][20] indicate that the topology of the model is UV dominated.

2 The model

The 2-d O(N) σ -models are O(N)-symmetric renormalizable quantum spin field theories, asymptotically free for $N \geq 3$.

They are described by the Lagrangian:

$$\mathcal{L} = \frac{\beta}{2} \partial_\mu \phi(x) \cdot \partial_\mu \phi(x) \quad , \quad (1)$$

where $\phi(x)$ is a N-component real field satisfying the constraint $\phi \cdot \phi = 1$ and β is the inverse of the coupling constant g .

The infrared charge singularity of these models is responsible for the disintegration of the Goldstone vacuum [21]; for $N \geq 3$ the true vacuum is O(N) symmetric and non-degenerate. In the limit $N \rightarrow \infty$ the model contains an isovector N-plet of free massive particles only [22][23]. The interaction of these particles is of order $1/N$ and so for N sufficiently large no bound states are present. Strong theoretical evidences bear the conjecture that the situation is the same at all $N \geq 3$ [24]. Consequently, the spectrum of the O(3) σ -model is expected to consist of a single triplet of particles.

Among the O(N) σ -models, the O(3) model in particular plays an important role in quantum field theory because it resembles, besides asymptotic freedom and spontaneous mass generation, another aspect of the 4-d non-Abelian gauge theories, i.e. the non-trivial topology.

The topological charge Q of a 3-component spin field $\phi(x)$ is the number of times $\phi(x)$ winds the sphere S^2 . It can be expressed as the integral over the space-time of a local operator $Q(x)$:

$$Q(x) = \frac{1}{8\pi} \epsilon_{\mu\nu} \epsilon_{ijk} \phi_i(x) \partial_\mu \phi_j(x) \partial_\nu \phi_k(x) \quad ; \quad (2)$$

$Q(x)$ is the divergence of a topological current K_μ [25][26],

$$Q(x) = \partial_\mu K_\mu(x) \quad . \quad (3)$$

All classical solutions with non-trivial topology – the k -instantons – have been explicitly found [27]. At a quantum level, the only available prediction comes from the semiclassical ap-

proximation; the 1-loop result³ for the size distribution of instantons in the physical vacuum is $(1/V)dN/d\rho \propto 1/\rho$. This expression gives a logarithmic divergence in the ultraviolet limit $\rho \rightarrow 0$. Moreover, numerical approaches for the evaluation of the instanton size distribution [19][20] indicate a growing behavior when the size decreases (the lowest size investigated is $\rho \sim 0.2 \xi_G$).

The topological susceptibility is defined as the correlation at zero momentum of two topological charge density operators $Q(x)$:

$$\chi = \int d^2x \langle 0 | T [Q(x)Q(0)] | 0 \rangle . \quad (4)$$

The prescription defining the product of operators in Eq. (4) is [28]

$$\langle 0 | T [Q(x)Q(0)] | 0 \rangle \equiv \partial_\mu \langle 0 | T [K_\mu(x)Q(0)] | 0 \rangle . \quad (5)$$

This prescription eliminates the contribution of possible contact terms (i.e. terms proportional to the δ function or its derivatives) when $x \rightarrow 0$.

3 Scaling: mass gap measurements

The general parametrization of the FP action of the O(3) σ -model is

$$A_{FP}(\phi) = \beta \left\{ -\frac{1}{2} \sum_{x,r} \rho(r) (1 - \phi(x) \cdot \phi(x+r)) \right. \\ \left. + \sum_{x_1, x_2, x_3, x_4} c(x_1, x_2, x_3, x_4) (1 - \phi(x_1) \cdot \phi(x_2)) (1 - \phi(x_3) \cdot \phi(x_4)) + \dots \right\}, \quad (6)$$

where ρ represents the perfect discretization of the Laplacian and all the (infinite) multi-spin couplings with more than 4 fields have been only implicitly indicated. In this paper we test the properties of the 24-couplings parametrization reported in Table 4 of Ref. [2], which contains only one-plaquette terms with no more than 8 fields.

This parametrized FP action should reproduce the continuum even at moderate values of the correlation length: cut-off effects on the spectral properties of the lattice theory should be absent, or at least strongly suppressed. This is confirmed by numerical evidences [2]. We want to check this point further.

We have performed our test by comparing alternative lattice definitions of mass gap. The

³Using the perturbative RG one can prove that this result is in fact asymptotically exact as $\rho \rightarrow 0$ [8].

standard definition is related with the large-distance behavior of the wall-wall correlation function⁴

$$G_w(y-x) = \frac{1}{L} \sum_{x_1, y_1} G(x_1, x; y_1, y) \quad , \quad (7)$$

where

$$G(x) = \langle \phi(x) \cdot \phi(0) \rangle \quad . \quad (8)$$

The expected large-distance behavior, including periodic boundary condition effects, is:

$$G_w(x) \simeq \frac{A_w}{2} \left[\exp\left(-\frac{x}{\xi_w}\right) + \exp\left(-\frac{L-x}{\xi_w}\right) \right] \quad \text{for } \frac{L}{2} > x \gg \xi_w \quad . \quad (9)$$

It is also possible to define the diagonal wall-wall correlation function

$$G_d\left(\frac{y-x}{\sqrt{2}}\right) = \frac{\sqrt{2}}{L} \sum_{x_1, y_1} G(x_1, x-x_1; y_1, y-y_1) \quad , \quad (10)$$

whose large-distance behavior is

$$G_d(x) \simeq \frac{A_d}{2} \left[\exp\left(-\frac{x}{\xi_d}\right) + \exp\left(-\frac{L/\sqrt{2}-x}{\xi_d}\right) \right] \quad \text{for } \frac{L}{2\sqrt{2}} > x \gg \xi_d \quad . \quad (11)$$

One of the scaling tests consists in verifying that the ratios ξ_d/ξ_w and A_d/A_w keep constant when β varies. In addition, the comparison between $\xi_d(A_d)$ and $\xi_w(A_w)$ allows to test directly the rotation invariance: scaling violations are revealed by deviations from 1 of the ratios ξ_d/ξ_w and A_d/A_w .

An alternative definition of the correlation length comes from considering the second moment of the correlation function

$$\xi_G^2 = \frac{\int d^2x \frac{1}{4} x^2 G(x)}{\int d^2x G(x)} \quad . \quad (12)$$

We use the following lattice definition of ξ_G :

$$\xi_G^2 = \frac{1}{4 \sin^2(\pi/L)} \left[\frac{\tilde{G}(0,0)}{\tilde{G}(0,1)} - 1 \right] \quad , \quad (13)$$

where $\tilde{G}(k)$ is the Fourier transform of $G(x)$, given by

$$\tilde{G}(k) = \frac{1}{L^2} \sum_{x,y} \langle \phi(x) \cdot \phi(y) \rangle \exp\left[i \frac{2\pi}{L} (x-y) \cdot k\right] \quad . \quad (14)$$

The zero component of $\tilde{G}(k)$ is by definition the magnetic susceptibility χ_m . In the scaling region the ratio ξ_G/ξ_w must be a constant, scale-independent number. The ratio should be equal to 1 within 1% [29].

⁴A small cut-off effect survives in the following definitions of the lattice mass gap since the ordinary lattice field ϕ instead of the FP field operator ϕ^{FP} is used [2][5].

Let's introduce the quantity $A_G = \chi_m \xi_G^{-2} \xi_w$. The adimensional ratio A_w/A_G is scheme-independent in the scaling region. We expect $A_w/A_G \approx 1$, because the two-point functions should be almost saturated by the lowest energy state.

We performed Monte Carlo (MC) simulations for several values of β corresponding to correlation lengths ξ varying from ~ 2 to ~ 34 lattice units. We adopted a 4-hits Metropolis algorithm which is the only local algorithm available for actions with multi-spin interactions. The local nature of the algorithm will be essential in the application of the heating techniques to be discussed later. The acceptance of the pseudo-random changes of the Monte Carlo has been adjusted at 50%.

In Table I we report values of correlation length and correlation function coefficient obtained, for the three definitions, at various β 's. The fits to G_w and G_d have been performed choosing $x_{min} \simeq \xi$; we have checked that larger values of x_{min} give results consistent within errors. Table II shows the ratios of these different definitions, analyzed using jackknife techniques. We can observe nice scaling and rotation invariance: in the region of β between 0.8 and 1.0 (ξ between ~ 5 and ~ 12) the uncertainty is lower than 1%. Moreover, with the same precision the ratios ξ_G/ξ_w and A_G/A_w are consistent with one, so confirming the picture of an $O(3)$ model with a one-particle spectrum (see the discussion in Section 2).

Table II shows also a test of asymptotic scaling, reporting the quantity $(\xi_G f(\beta)_{2l})^{-1}$, where $f(\beta)_{2l} = 2\pi\beta e^{-2\pi\beta}$ is the 2-loop renormalization group function. In the asymptotic scaling region this quantity should be constant. However, numerical outcomes exhibit a steady growth and, moreover, they are far from the theoretical value $M_G/\Lambda_{FP} = 9.802494$ (Λ_{FP} is the Λ parameter of the theory regularized with the FP action) coming from the exact result for M_G of Ref. [30] and from the relation $\Lambda_{FP} = 8.17 \Lambda_{ST}$ [2]. We stress that this is not in contradiction with the properties of the FP action which do manifest only in the physical scaling of the lattice theory. Our hypothesis is that the deviation from asymptotic scaling is due to large non-universal corrections in the function $f(\beta)$. We have fitted data in the seventh column of Table II taking into account the first non-universal correction: $f_{3l}(\beta) = f(\beta)_{2l}(1 + \delta/(2\pi\beta))$. Imposing for M_G/Λ_{FP} the previously quoted theoretical value, we find $\delta = -1.746(23)$, $\chi^2/\text{d.o.f.} \simeq 0.8$. The higher order corrections to $f(\beta)_{2l}$ are non-negligible in the region of β accessible to Monte Carlo simulations and it is essential to include them when the scaling of physical quantities is studied with this kind of action. Involving in the fit procedure also the ratio M_G/Λ_{FP} , we find $M_G/\Lambda_{FP} = 9.97(5)$, $\delta = -1.80(3)$, $\chi^2/\text{d.o.f.} \simeq 0.9$. Nevertheless, we observe that the uncertainty of this measure is much larger than the naïve error of the fit here quoted. A more reliable error can be found by checking the stability of the result under various alternative fits. Our conclusion is that the real uncertainty is about 10%, being therefore our determination of M_G/Λ_{FP} compatible with the prevision of Ref. [30].

4 Stability of lattice classical configurations

When instantons are discretized on the lattice, generally their action is no more scale invariant. In the case of the standard lattice action, for instance, the action of instantons decreases with their size [8] and, as a consequence, instantons are not stable under local minimization of the action, but shrink up to destruction [9].

The FP action is scale invariant [2] (up to a minimum size [13]) and so its topological classical solutions are stable under minimization. When a parametrized form of the FP action is used in numerical simulations the statement about stability of instantons becomes likely approximate: however, a huge improvement is expected with respect to the standard action, and with respect to the tree level Symanzik improved action [1] too, where only $\mathcal{O}(a^2)$ cut-off effects are removed.

Anyway, we did not study the absolute stability of instantons under minimization, our main interest being to check to what extent a fixed (finite) number of steps of local minimization modifies the lattice topological structures. This is a way to have control over the loss of topological signal which affects the lattice determination of the topological susceptibility by cooling techniques [9][16] (see Section 7).

In view of this, we have discretized on a 60^2 lattice the exact 2-instanton continuum solution defined on a torus [18]⁵ (1-instantons do not exist on a torus [18][19]). The study consisted in the observation of the behavior during 100 steps of cooling of both the topological charge and the action of the discretized 2-instanton. We studied 2-instantons of size⁶ ranging from $0.2a$ to $5a$, comparing the performances of the FP and tree level Symanzik improved actions. We have adopted an improved version of the lattice charge operator (see Section 7). The local minimization of the lattice action was obtained by making use of the Metropolis algorithm in the usual fashion, but with the request that only upgradings which lower the action are accepted. A sweep of this $\beta = \infty$ Metropolis is a cooling step. As a preliminary task we have checked that the efficiency of the algorithm of minimization is independent of the action; this test has been realized by cooling lattice configurations with trivial topology, and verifying that the behavior of charge and action is similar in the two cases.

The results of the study on the 2-instanton are summarized in Figs. 1 and 2. We observe that in the case of the FP action topological charge loss is tiny if the size of the 2-instanton is larger than $0.9a$. For size smaller than $0.9a$ the discretized configuration becomes unstable and it is destroyed by few cooling steps. The deviation from 2 of the topological charge of the cooled instantons with size smaller than $3a$ is explained by a residual scale dependence of our (only partially improved)

⁵We thank M. Blatter and R. Burkhalter for many helpful suggestions in this regard.

⁶The size is defined as in the case of instantons on the sphere [17].

definition of the lattice charge operator. In the case of the Symanzik action qualitatively the same behavior is observed, with the important difference that the topological signal is almost totally lost already at size $1.5a$.

A detailed analysis of the behavior of the charge during the cooling procedure gives some indications about shrinking effects. Shrinking can be observed in both the Symanzik and parametrized FP actions, increasing at small sizes (where the scale symmetry breaking of the discretization is amplified); however, it is much reduced in the case of the FP action (see Table III): at $\rho = 2a$, for instance, it is ~ 2 orders of magnitude smaller.

In Fig. 3 we compare the different cooling shapes of a small-size 2-instanton ($\rho = 1.2a$) when the FP, the standard and the Symanzik actions are used; being the algorithm of minimization non-deterministic, we have checked to what extent results fluctuate under changing of the sequences of random numbers used in the minimization algorithm.

Although single-instanton classical solutions are not allowed on a torus, it is nevertheless interesting to investigate the amount of topological loss under cooling in the $Q = 1$ topological charge sector, which is dominant among classical configurations at thermal equilibrium. It is impossible to perform a study strictly equivalent to the previous one in the $Q=2$ sector, because 1-instanton solutions are missing on a torus: in their place, we have used 1-instanton solutions with constant boundary conditions [27] which are quasi-solutions for $\rho/L \ll 1$ (L is the lattice size). We have found substantially the same results of Figs. 1 and 2 as far as the minimum sizes are concerned: the main difference is that the observed action is slightly above the expected value 4π at large ρ , going asymptotically to 4π when ρ/L decreases (in Fig. 4 we report the results for the FP action); clearly this is a boundary effect (the configuration does not satisfy the correct periodic boundary conditions).

5 Topology: the geometrical method

In this Section we check how the geometrical method for the determination of the topological susceptibility [7] works when the FP action is used.

The geometrical definition Q_g of the lattice topological charge is an attempt to recover the topological structure of the continuum theory by interpolating the discrete lattice field with a continuous field on which the topological charge can be measured. In formulae:

$$Q_g = \sum_{x^*} q(x^*) \quad , \quad (15)$$

where x^* indicates a vertex of the dual lattice (corresponding to a plaquette of the 2-d lattice)

and

$$q(x^*) = \frac{1}{4\pi} \{(\sigma A)(\phi_1, \phi_2, \phi_3) + (\sigma A)(\phi_1, \phi_3, \phi_4)\} \quad . \quad (16)$$

$\phi_1, \phi_2, \phi_3, \phi_4$ are the four spins belonging to the plaquette x^* and $(\sigma A)(\phi_1, \phi_2, \phi_3)$ denotes the signed area of the spherical triangle ϕ_1, ϕ_2, ϕ_3 ⁷.

The topological susceptibility constructed in terms of the geometrical charge $\chi_g = \langle Q_g^2/V \rangle$ [7] fails to reproduce the correct continuum behavior: the reason is that the geometrical definition assigns non-zero topological charge to lattice structures of unphysical size (dislocations). In the case of the standard lattice action, dislocations proliferate in the $\beta \rightarrow \infty$ limit [8][9] since their action is definitely lower than 4π , the minimal (physical) value in the $Q = 1$ sector. As a consequence, they produce a non-scaling topological signal. Now, it is interesting to investigate to what extent the situation improves with the FP action, checking, in particular, if dislocations are still present and, if so, if their action is at least closer to 4π . In order to have an indication about this subject, we have studied the cooling of a discretized 1-instanton solution (with constant boundary solutions to infinity). This lattice configuration – which is not a local minimum of the action on a toroidal lattice – is driven by the cooling algorithm to the nearest minimum in the $Q_g = 1$ sector (lying on the border between the $Q_g = 1$ to the $Q_g = 0$ sectors), and eventually it passes into the $Q_g = 0$ sector. The action of this border configuration is, in the case at hand (see Fig. 5), $S/4\pi = 0.92 < 1$, thus indicating a dislocation. This outcome (though the method was not rigorous) suggests that the action of dislocations is closer to 4π compared to the case of the standard action, where the minimal action in the $Q_g = 1$ sector is 0.53 [8]. Anyway, dislocations are still present, so, apart from non-scaling effects due to the UV topological dominance of the model [19][20], a deviation of χ_g from the renormalization group behavior is expected.

We have performed numerical simulations on χ_g (see Fig. 6 and Table IV) finding $\chi_g \sim \beta^2 e^{-4\pi\alpha\beta}$, with $\alpha = 0.8315(11)$, $\chi^2/\text{d.o.f.} \simeq 0.8$. For comparison, we report the α coefficient obtained in the case of the standard action [7], $\alpha = 0.625$: clearly the effect of dislocations is lower with the FP action.

6 Topology: the field theoretical method

⁷One can demonstrate that

$$\begin{aligned} \exp\left(\frac{1}{2}i\sigma A\right) &= \rho^{-1} \{1 + \phi_1 \cdot \phi_2 + \phi_2 \cdot \phi_3 + \phi_3 \cdot \phi_1 + i\phi_1 \cdot (\phi_2 \times \phi_3)\} \quad , \\ \rho &= \{2(1 + \phi_1 \cdot \phi_2)(1 + \phi_2 \cdot \phi_3)(1 + \phi_3 \cdot \phi_1)\}^{1/2} > 0 \quad , \end{aligned} \quad (17)$$

thus providing an explicit formula for Q_g .

6.1 Perturbative calculations

We follow the field theoretical method [15] for the determination of the topological susceptibility from the lattice. First of all, a lattice topological charge density operator is defined as a local operator having the appropriate classical continuum limit [31]; our choice is [12]:

$$Q^L(x) = \frac{1}{32\pi} \epsilon_{\mu\nu} \epsilon_{ijk} \phi_i(x) (\phi_j(x + \mu) - \phi_j(x - \mu)) (\phi_k(x + \nu) - \phi_k(x - \nu)) \quad . \quad (18)$$

From the prescriptions of field theory it comes that a finite multiplicative renormalization connects the matrix elements of the lattice topological charge density with those of its continuum counterpart:

$$Q^L(x) = a^2 Z(\beta) Q(x) + O(a^4) \quad . \quad (19)$$

We recall: $\beta = 1/g$. The lattice-regularized version of χ is

$$\chi^L = \left\langle \sum_x Q^L(x) Q^L(0) \right\rangle = \frac{1}{L^2} \left\langle \left(\sum_x Q^L(x) \right)^2 \right\rangle \quad , \quad (20)$$

where L is the lattice size.

A prescription equivalent to Eq. (5) does not exist on the lattice and therefore the contribution of the contact terms must be isolated and subtracted. These contact terms appear as mixings with the action density $S(x)$ and with the unity operator I , which are the only available operators with equal dimension or lower. In formulae

$$\chi^L(\beta) = a^2 Z(\beta)^2 \chi + a^2 A(\beta) \langle S(x) \rangle + P(\beta) \langle I \rangle + O(a^4) \quad . \quad (21)$$

In Eq. (21) the quantity $\langle S(x) \rangle$ is intended to be the non-perturbative part of the expectation value of the action density, i.e. it is a signal of dimension two.

The extraction of the physical value of the topological susceptibility from numerical simulations requires the evaluation of the renormalization constants $Z(\beta)$, $A(\beta)$, $P(\beta)$.

The standard way to proceed is to perform the calculation in perturbation theory. We have decided to consider in our calculations the quartic terms of the parametrization of the FP action with coefficient $\mathcal{O}(10^{-2})$ or larger. The procedure followed for the calculation of $Z(\beta)$ and $P(\beta)$ is illustrated in Ref. [12]; for $A(\beta)$ we refer to Ref. [20].

An intermediate step in the calculation of $Z(\beta)$ is the evaluation of the renormalization constants of the fields $\pi(x)$ and of the coupling constant g . We have found them to 1-loop order by imposing

$$Z_\pi^{\overline{MS}}(g, \mu a) \Gamma_{\pi\pi}^L(g, h, a; p) = \Gamma_{\pi\pi}^{\overline{MS}}(g_r, h_r, \mu; p) \quad , \quad (22)$$

where $g = Z_g^{\overline{MS}} g_r$, $h = Z_g^{\overline{MS}} Z_\pi^{\overline{MS}-1/2} h_r$. We quote here the results:

$$\begin{aligned} Z_\pi^{\overline{MS}}(g, \mu a) &= 1 - 2L(\mu a)g + O(g^2) \ , \\ Z_g^{\overline{MS}}(g, \mu a) &= 1 - (L(\mu a) + c_1)g + O(g^2) \ , \end{aligned} \quad (23)$$

where $L(x) = -\frac{1}{2\pi} \ln x + \frac{5}{4\pi} \ln 2 - y$, being $y = 0.0382$ and $c_1 = 0.1262$. We observe that at this order $Z_\pi^{\overline{MS}}$ is independent from the couplings of the multi-spin terms which affect only c_1 .

For the calculation of $Z(\beta)$ we compare the 2-point Γ -functions with one operator insertion on the lattice and on the continuum:

$$Z(\beta)^{-1} Z_\pi^{\overline{MS}}(g, \mu a) \Gamma_{Q, \pi\pi}^L(g, h, a; p, q) = \Gamma_{Q, \pi\pi}^{\overline{MS}}(g_r, h_r, \mu; p, q) \ . \quad (24)$$

$\Gamma_{Q, \pi\pi}$ does not take contribution from the couplings of multi-spin terms at 1-loop order, so our 1-loop determination of $Z(\beta)$ is exact. We show the result:

$$Z(\beta) = 1 + \frac{z_1}{\beta} + O(\beta^{-2}) \ , \quad z_1 = -0.94237 \ . \quad (25)$$

We calculated the perturbative tail $P(\beta) = \sum_{n=4} p_n / \beta^n$ up to four loops. The results for infinite volume are:

$$p_4 = 1.97429 \times 10^{-4} \ , \quad p_5 = -2.24879 \times 10^{-4} \ . \quad (26)$$

Only p_5 is affected by our approximation. These numbers were extracted by performing numerical integrations at finite volume and extrapolating the results to infinite volume.

We have calculated the a_3 coefficient in the perturbative series $A(\beta) = \sum_{n=3} a_n / \beta^n$ by comparing $\Gamma_{(Q^L)^2/V, \pi\pi}$ with $\Gamma_{S, \pi\pi}$ at the lowest order (for details see the Appendix in Ref. [20]). The value of a_3 extrapolated to infinite volume is 7.76206×10^{-4} . This result also is independent from the multi-spin terms. As in the case of the tree level Symanzik improved action [20], the mixing of the topological susceptibility with the action density is absolutely irrelevant.

6.2 Numerical simulations

We have performed Monte Carlo simulations for χ^L on a 60^2 lattice over an extended region of values of β , the algorithm being the same 4-hits Metropolis of previous simulations. In Table V we report the results: binning techniques have been applied in order to take account of the effect of correlations in the evaluation of errors. In order to control finite size effects, we have repeated the simulations at $\beta = 1.0, 1.1, 1.2$ with the care that $L/\xi_G \sim 6$. We observe (see Table V) that only the datum at $\beta = 1.2$ appreciably differs from the result on the 60^2 lattice.

In the range of values of β accessible to our lattices, the perturbative determinations of the previous subsection are not sufficient to have a reliable estimate of the renormalizations $Z(\beta)$ and $P(\beta)$. Moreover, the standard technique to estimate some further terms in the perturbative expansion of $P(\beta)$ by a fit on numerical data at β higher than a certain β_t (the so-called perturbative region) does not work: the extrapolation of $P(\beta)$ to lower values of β , where the physical signal is still living, is not reliable, since this procedure is unstable under changes of the conditions of the fit. So, we followed an alternative method for the determination of the renormalizations of the lattice topological susceptibility: the “heating” method [32][33]. The heating method, relying only on MC techniques, is fully non-perturbative. It consists (for details see also [12][20]) in constructing on the lattice ensembles of configurations $\{C_t\}$, each configuration of the ensemble being obtained by performing a sequence of t local Monte Carlo sweeps starting from a discretized classical configuration C_0 – a large instanton or the flat configuration. For small t , the heating process thermalizes only the small-range fluctuations which are responsible for the renormalizations: when the starting configuration is a large instanton (flat configuration), measuring $Q^L(\chi^L)$ on the ensembles $\{C_t\}$, a plateau at the value of $Z(\beta)$ ($P(\beta)$) is observed after a certain time, not depending on β , corresponding to the thermalization of quantum fluctuations.

In Table VI we show the values of $Z(\beta)$ evaluated by the heating procedure at various β . Data reported therein have been obtained by heating a discretized 1-instanton with constant boundary conditions⁸ (size 10 lattice units) on a 60^2 lattice. The ensembles $\{C_t\}$ have been obtained performing t sweeps of the Metropolis algorithm. In Table VI we also compare the non-perturbative determinations of $Z(\beta)$ with our 1-loop perturbative calculation: the latter well reproduces the non-perturbative results at the largest values of β , but a deviation is observed at the smallest ones, where the 1-loop perturbative expansion is expected to fail. Attributing this discrepancy to the next-to-leading terms of the perturbative expansion of $Z(\beta)$, we have found by a fit on data for $\beta \leq 1.4$: $z_2 = 0.473(7)$, $z_3 = -0.234(9)$ ($\chi^2/\text{d.o.f.} \simeq 0.1$).

In Table VII we show the outcomes of the heating method for $P(\beta)$ at various β . Data have been obtained on a 60^2 lattice. Using data from heating, we have fitted two further coefficients, p_6 and p_7 , of the perturbative expansion of $P(\beta)$; the result is: $p_6 = (7.54 \pm 0.09) \times 10^{-5}$, $p_7 = (3.02 \pm 0.10) \times 10^{-5}$, with $\chi^2/\text{d.o.f.} \simeq 0.9$. In Fig. 7 we compare three different determinations of $P(\beta)$: the first is the pure 4-loop perturbative calculation; the second is a fit which combines the perturbative calculation with the equilibrium values of χ^L at values of β larger than 1.6; the last is the non-perturbative determination of $P(\beta)$. As it can be clearly observed, the curve from the second determination badly reproduces data from the heating method for the values of β not included in the fit, i.e. $\beta < 1.6$. This explains why the standard procedure of extracting the perturbative tail joining perturbative calculations and MC data from the perturbative region fails in this case.

⁸For the purposes of this method it is sufficient to thermalize around any smooth configuration with non-trivial topology.

Having obtained a reliable determination of the renormalizations $Z(\beta)$ and $P(\beta)$, we are now in a position to extract from χ^L the physical quantity χ (see Eq. (21) – the term proportional to $A(\beta)$ is negligible).

In Table VIII (see also Fig. 8) we report, for different values of β , the quantities χ/Λ_{FP}^2 and χ/M_G^2 (in the latter entry we use the relation between Λ_{FP} and M_G which can be deduced from Ref. [30]); we also report our determination of ξ_G , as obtained from the fit of Section 3 (the one with the ratio M_G/Λ_{FP} fixed at the theoretical value of Ref. [30]).

In Table IX we compare our present results for χ/M_G^2 with other determinations known in literature. Data in columns (2) and (3) have been obtained in the field theoretical approach with the standard definition of the topological charge operator, but using other lattice regularizations of the action [12][34]. In column (4) a parametrized FP action and the FP lattice charge operator have been used. The FP charge operator has been constructed by the application of one RG transformation on the geometrical charge operator [13]. A substantial agreement is observed among determinations using the standard charge operator in the field theoretical approach, while data for χ/M_G^2 of column (4), where a FP charge operator is used, are systematically larger. We argue that the disagreement originates from the different performance in the short distance regime of the two lattice definitions of the charge operator. Indeed, the field theoretical definition is likely to underestimate the topological content of small size topological configurations (as Fig. 1 clearly singles out), while such loss of topological signal is definitely less relevant with the FP operator of Ref. [13] (Fig. 2 of the previously quoted reference). This different behavior strongly reflects upon the determination of the topological susceptibility, owing to the UV topological dominance of the model.

7 Topology: the cooling method

In this Section we turn to an alternative way to face the matter of renormalizations, known in literature as the cooling method [9][16]. The method relies on a local algorithm of minimization of the action of lattice configurations – the cooling; the purpose is to destroy the quantum fluctuations of the lattice configuration generated by the MC algorithm (which give rise to the renormalizations $Z(\beta)$ and $P(\beta)$ of Eq. (21)), trying to preserve the background topological structure. If the background structure is an extended classical configuration, after a large enough number of cooling iterations, a measure of the lattice topological charge on the cooled configuration well approximates an integer⁹.

⁹If the background configuration is not slowly varying, scale effects produce deviations from integer values, due to the scale dependence of the field theoretical charge operator (see Section 4).

As we have seen in Section 4, shrinking effects are tiny with the (parametrized) FP action, so the most important drawback of the cooling procedure is overcome.

In Table V we report the results of the simulations on a 60^2 lattice. The minimization algorithm has been described in Section 4; the “cooled” equilibrium value of the topological susceptibility has been determined by measuring the topological charge on configurations obtained from the equilibrium ones after 30 iterations of the algorithm.

Here we adopt a different definition of the lattice charge operator. It consists in a tree level Symanzik improved operator, where the first three irrelevant terms have been eliminated:

$$Q^L(x) = \frac{1}{8\pi} \epsilon_{\mu\nu} \epsilon_{ijk} \phi_i(x) D_\mu \phi_j(x) D_\nu \phi_k(x) \quad ; \quad (27)$$

D_μ is the improved lattice derivative:

$$D_\mu = \frac{1225}{1024} \nabla_\mu^{(1)} - \frac{245}{1024} \nabla_\mu^{(3)} + \frac{49}{1024} \nabla_\mu^{(5)} - \frac{5}{1024} \nabla_\mu^{(7)} \quad , \quad (28)$$

$$\nabla_\mu^{(n)} \phi_i(x) = \frac{1}{2n} (\phi_i(x + n\mu) - \phi_i(x - n\mu)) \quad .$$

Being the first irrelevant terms absent, this operator is less sensitive to quantum fluctuations than the definition of Eq. (18) and, as a consequence, the determination of the topological charge of the cooled configurations improves.

For each value of β typically 100000 configurations were generated, the cooling procedure being performed once every 100 configurations. In Table VIII and in Fig. 8 we compare the cooling determinations with the results of the field theoretical method. Data from cooling nicely reproduce the outcomes of the field theoretical method, so confirming that topological structures are affected in a negligible way by the cooling procedure.

The results for χ/M_G^2 obtained on large lattices by cooling (see Table VIII) allow now to appreciate a slight deviation from scaling – a non-scaling behavior is observed also in Ref. [13]. Such deviation is expected since a (β -dependent) part of the whole topological signal is lost on the lattice due to the UV dominance of the model. However, the discrepancy of our data with the results of the previously quoted reference is still present and so it cannot be explained by finite size effects.

Acknowledgments. We wish to thank Adriano Di Giacomo for having suggested the subject, M. Blatter, R. Burkhalter, A. Hasenfratz, P. Hasenfratz, F. Niedermayer, P. Rossi and E. Vicari for many useful discussions. This work was partially supported by Fondazione “A. Della Riccia” (Italy).

References

- [1] K. Symanzik, *in* Recent developments of gauge theories, ed. G. 't Hooft et al. (Plenum, New York, 1980); *in* Lecture Notes in Physics, 153, ed. R. Schrader et al. (Springer, Berlin, 1982); *in* Non-perturbative field theory and QCD, ed R. Jengo et al. (World Scientific, Singapore, 1983);
K. Symanzik, Nucl. Phys. **B226** (1983) 187 and 205;
B. Berg, I. Montvay and S. Meyer, Nucl. Phys. **B235**[FS11] (1984) 149;
G. Martinelli, G. Parisi and R. Petronzio, Phys. Lett. **B100** (1981) 485;
G. Parisi, Nucl. Phys. **B254** (1985) 58;
P. Weisz, Nucl. Phys. **B212** (1983) 1;
P. Weisz and R. Wohlert, Nucl. Phys. **B236** (1984) 397;
G. Curci, P. Menotti and G. Paffuti, Phys. Lett. **B130** (1983) 205;
B. Berg, A. Billoire, S. Meyer and C. Panagiotakopoulos, Comm. Math. Phys. **97** (1985) 31;
M. Falcioni, G. Martinelli, M.L. Paciello, G. Parisi and B. Taglienti, Nucl. Phys. **B225**[FS9] (1983) 313;
M. Lüscher and P. Weisz, Comm. Math. Phys. **97** (1985) 59;
M. Lüscher and P. Weisz, Nucl. Phys. **B240**[FS12] (1984) 349;
B. Sheikholeslami and R. Wohlert, Nucl. Phys. **B259** (1985) 572.
- [2] P. Hasenfratz and F. Niedermayer, Nucl. Phys. **B414** (1994) 785; P. Hasenfratz, Nucl. Phys. **B** (Proc. Suppl.) **34** (1994) 3; F. Niedermayer, *ibid.* 513.
- [3] K.G. Wilson and J. Kogut, Phys. Rep. **C12** (1974) 75;
K.G. Wilson, Rev. Mod. Phys. **47** (1975) 773; *ibid.* **55** (1983) 583.
- [4] K.G. Wilson, *in* Recent developments of gauge theories, ed. G. 't Hooft et al. (Plenum, New York, 1980).
- [5] T. DeGrand, A. Hasenfratz, P. Hasenfratz and F. Niedermayer, preprint COLO-HEP-361, BUTP-95/14, (1995).
- [6] F. Farchioni, P. Hasenfratz, F. Niedermayer and A. Papa, preprint BUTP-95/16, IFUP-TH 33/95, (1995).
- [7] B. Berg and M. Lüscher, Nucl. Phys. **B190**[FS3] (1981) 412.
- [8] M. Lüscher, Nucl. Phys. **B200**[FS4] (1982) 61.
- [9] B. Berg, Phys. Lett. **B104** (1981) 475.
- [10] G. Martinelli, R. Petronzio and M.A. Virasoro, Nucl. Phys. **B205**[FS5] (1982) 355.
- [11] B. Berg and C. Panagiotakopoulos, Nucl. Phys. **B251**[FS13] (1985) 353.

- [12] A. Di Giacomo, F. Farchioni, A. Papa and E. Vicari, Phys. Rev. **D46** (1992) 4630; Phys. Lett. **B276** (1992) 148.
- [13] M. Blatter, R. Burkhalter, P. Hasenfratz and F. Niedermayer, Nucl. Phys. **B** (Proc. Suppl.) **42** (1995) 799.
- [14] B. Allés and M. Beccaria, ‘The 2–dimensional non–linear σ –model on a random lattice’, Pisa preprint, IFUP–TH 11/95, hep–lat/9503025.
- [15] M. Campostrini, A. Di Giacomo and H. Panagopoulos, Phys. Lett. **B212** (1988) 206;
M. Campostrini, A. Di Giacomo, H. Panagopoulos and E. Vicari, Nucl. Phys. **B329** (1990) 683; Nucl. Phys. **B** (Proc. Suppl.) **17** (1990) 634;
M. Campostrini, A. Di Giacomo, Y. Gündüç, M.P. Lombardo, H. Panagopoulos and R. Tripic-
cione, Phys. Lett. **B252** (1990) 436.
- [16] M. Teper, Phys. Lett. **B171** (1986) 81 and 86.
- [17] A. Jevicki, Nucl. Phys. **B127** (1977) 125;
D. Förster, Nucl. Phys. **B130** (1977) 38;
B. Berg and M. Lüscher, Comm. Math. Phys. **69** (1978) 57;
V.A. Fateev, I.V. Frolov and A.S. Schwarz, Nucl. Phys. **B154** (1979) 1.
- [18] J.–L. Richard and A. Rouet, Nucl. Phys. **B211** (1983) 447.
- [19] C. Michael and P.S. Spencer, Phys. Rev. **D50** (1994) 7570.
- [20] F. Farchioni and A. Papa, Nucl. Phys. **B431** (1994) 686.
- [21] E. Brezin, J. Zinn–Justin and J.C. Le Guillou, Phys. Rev. **D14** (1976) 2615.
- [22] E. Brezin and J. Zinn–Justin, Phys. Rev. **B14** (1976) 3110.
- [23] W.A. Bardeen, B.W. Lee and L.E. Shrock, Phys. Rev. **D14** (1976) 985.
- [24] A.B. Zamolodchikov and A.B. Zamolodchikov, Nucl. Phys. **B133** (1978) 525; Ann. of Phys. **120** (1979) 253.
- [25] G. ’t Hooft, Phys. Rev. Lett. **37** (1976) 8; Phys. Rev. **D14** (1976) 3432.
- [26] A. D’Adda, P. Di Vecchia and M. Lüscher, Nucl. Phys. **B146** (1978) 63.
- [27] A.A. Belavin and A.M. Polyakov, JETP Lett., Vol. **22**, No. 10 (1975) 245.
- [28] R. J. Crewther, Nuovo Cimento, Rev. series 3, Vol. **2**, (1979) 8.
- [29] M. Campostrini and P. Rossi, Phys. Lett. **B272** (1991) 305.
- [30] P. Hasenfratz, M. Maggiore and F. Niedermayer, Phys. Lett. **B245** (1990) 522.

- [31] P. Di Vecchia, K. Fabricius, G. C. Rossi and G. Veneziano, Nucl. Phys. **B192** (1981) 392;
K. Ishikawa, G. Schierholz, H. Schneider and M. Teper, Phys. Lett. **B128** (1983) 309.
- [32] M. Teper, Phys. Lett. **B232** (1989) 227.
- [33] A. Di Giacomo and E. Vicari, Phys. Lett. **B275** (1992) 429.
- [34] M. Campostrini, P. Rossi and E. Vicari, Phys. Rev. **D46** (1992) 2647.

TABLE I: correlation length ξ and correlation function coefficient A with the FP action.

β	L	ξ_G	ξ_w	ξ_d	A_G	A_w	A_d
0.6	36	2.14(4)	2.188(15)	2.180(21)	5.15(18)	4.84(4)	4.84(6)
0.7	36	3.14(5)	3.16(5)	3.17(5)	6.3(1)	6.22(11)	6.19(12)
0.75	36	3.89(7)	3.89(7)	3.89(6)	7.04(7)	6.96(12)	7.00(9)
0.8	36	4.81(7)	4.83(9)	4.80(6)	8.103(23)	8.01(14)	8.11(8)
0.85	36	5.87(9)	5.86(13)	5.97(9)	9.37(3)	9.45(17)	9.30(10)
0.9	48	7.34(16)	7.34(21)	7.34(15)	10.98(3)	10.99(25)	11.12(14)
1.0	48	11.71(29)	11.8(4)	11.89(27)	15.01(14)	15.0(3)	15.4(3)
1.1	130	18.5(2.1)	18.1(2.7)	19.1(2.1)	22.3(4)	24(4)	22.2(1.7)
1.15	150	24.4(1.9)	24.3(2.5)	23.7(1.6)	26.5(3)	26.7(2.5)	28.2(1.2)
1.2	150	34(3)	34(4)	33.0(2.9)	33.1(1.3)	32(3)	35.1(2.6)

TABLE II: ratios of different definitions of correlation length and correlation function coefficient; in the last column we show $(\xi_G f(\beta)_{2l})^{-1}$.

β	L	ξ_G/ξ_w	ξ_d/ξ_w	A_w/A_G	A_d/A_w	$(\xi_G f(\beta)_{2l})^{-1}$
0.6	36	0.976(18)	0.997(7)	0.94(3)	1.001(11)	5.59(23)
0.7	36	0.994(5)	1.003(9)	0.987(11)	0.996(17)	5.88(10)
0.75	36	0.9977(21)	0.998(11)	0.988(9)	1.006(18)	6.08(11)
0.8	36	0.997(4)	0.994(11)	0.989(14)	1.011(19)	6.28(9)
0.85	36	1.002(6)	1.019(15)	1.009(19)	0.984(22)	6.66(11)
0.9	48	1.000(6)	0.999(18)	1.001(22)	1.012(27)	6.88(16)
1.0	48	0.993(12)	1.008(25)	1.00(3)	1.03(3)	7.28(18)
1.1	130	1.02(4)	1.06(11)	1.09(15)	0.91(15)	7.8(9)
1.15	150	1.00(3)	0.98(6)	1.01(10)	1.05(10)	7.8(6)
1.2	150	0.99(5)	0.96(10)	0.97(13)	1.09(16)	7.5(6)

TABLE III: topological charge (in the field theoretical definition) of 2-instantons of different initial size at the beginning and after 100 step of the cooling procedure with the Symanzik and the FP actions. The lattice size is 60.

ρ/a	Q_0	Q_{100}	
		Symanzik action	FP action
4	1.99856751	1.99856600	1.99856713
2	1.93896373	1.92357210	1.93858846
1.2	1.64901344	0.00001479	1.64991933

TABLE IV: χ_g , χ_g/Λ_{FP}^2 and χ_g/M_G^2 for various β and ξ_G on a 60^2 lattice. ξ_G is obtained from the fit of Section 3 (the one with the ratio M_G/Λ_{FP} fixed at the theoretical value of Ref. [30]).

β	ξ_G	$\chi_g \times 10^4$	χ_g/Λ_{FP}^2	χ_g/M_G^2
1.05	15.42(7)	8.27(26)	18.9(8)	0.197(8)
1.1	19.82(9)	5.63(21)	21.2(1.0)	0.221(10)
1.15	25.58(11)	3.61(9)	22.7(8)	0.236(8)
1.2	33.13(13)	2.25(7)	23.7(9)	0.247(10)

TABLE V: χ^L and χ_{cool} versus β on a 60^2 lattice. Data with *, **, and *** are obtained on lattices 70^2 , 130^2 and 180^2 , respectively.

β	$\chi^L \times 10^5$	$\chi_{cool} \times 10^4$	β	$\chi^L \times 10^5$
0.8	27.0(4)	-	1.5	1.91(6)
0.85	23.8(3)	-	1.52	1.94(9)
0.9	20.30(29)	-	1.55	1.77(8)
0.95	17.13(18)	9.2(5)	1.58	1.61(7)
1.	14.12(16)	6.42(29)	1.6	1.54(5)
*1.	13.97(20)	5.98(27)	1.65	1.39(6)
1.05	11.28(12)	4.48(21)	1.7	1.23(5)
1.1	9.18(10)	2.79(19)	1.75	1.06(6)
**1.1	9.48(25)	2.9(3)	1.8	0.98(5)
1.12	8.01(9)	2.35(13)	2.	0.68(3)
1.14	7.36(9)	1.88(11)	2.2	0.487(15)
1.16	6.72(8)	1.48(9)	2.3	0.426(14)
1.18	6.05(8)	1.33(10)	2.5	0.326(10)
1.2	5.42(6)	1.00(9)	2.8	0.199(6)
***1.2	6.75(25)	1.27(13)	3.	0.160(5)
1.22	5.3(3)	-	3.5	0.095(3)
1.225	4.91(22)	-	4.	0.0576(9)
1.25	4.50(17)	-	4.5	0.0384(10)
1.3	3.82(15)	-	5.	0.0256(7)
1.32	3.35(10)	-	6.	0.0131(9)
1.35	3.06(15)	-	7.	0.00683(18)
1.38	2.96(15)	-	8.	0.00409(11)
1.4	2.72(23)	-	9.	0.00250(7)
1.42	2.40(7)	-	10.	0.00178(5)
1.45	2.36(18)	-		

TABLE VI: $Z(\beta)$ versus β . $Z(\beta)_{1l}$ is the multiplicative renormalization calculated to one loop. $Z(\beta)_{MC}$ is the multiplicative renormalization calculated by heating a discretized $Q = 1$ smooth configuration; the size of the lattice is 90 for $\beta \geq 1.5$ and 60 for the remainder; the statistic of the simulations is 1000. Since data on the plateau are correlated, we have estimated errors by jackknife techniques.

β	$Z(\beta)_{1l}$	$Z(\beta)_{MC}$
5.0	0.812	0.8247(7)
4.5	0.791	0.8096(8)
4.0	0.746	0.7865(11)
3.5	0.731	0.7599(13)
3.0	0.686	0.7254(18)
2.5	0.623	0.6804(25)
2.1	0.551	0.631(3)
1.9	0.504	0.591(4)
1.7	0.446	0.566(4)
1.5	0.372	0.514(6)
1.4	0.327	0.479(9)
1.35	0.302	0.466(10)
1.3	0.275	0.450(10)
1.25	0.246	0.430(11)
1.2	0.215	0.406(12)
1.15	0.181	0.380(13)
1.1	0.143	0.362(14)

TABLE VII: $P(\beta)_{np}$ versus β . $P(\beta)_{np}$ is the mixing with the unity operator I calculated by heating the flat configuration; the size of the lattice is 60, the statistic of the simulation is 1000.

β	$P(\beta)_{np} \times 10^5$	β	$P(\beta)_{np} \times 10^5$
1.	7.58(24)	1.25	3.30(8)
1.05	6.48(19)	1.3	2.84(6)
1.1	5.49(14)	1.35	2.53(6)
1.15	4.60(11)	1.4	2.23(5)
1.2	3.84(9)		

TABLE VIII: χ/Λ_{FP}^2 and χ/M_G^2 for various β and ξ_G for both the field theoretical and the cooling determinations. L is the size of the lattice.

β	L	ξ_G	χ/Λ_{FP}^2	χ/M_G^2	$\chi_{cool}/\Lambda_{FP}^2$	χ_{cool}/M_G^2
0.8	60	4.74(3)	8(7)	0.09(7)	-	-
0.85	60	5.92(4)	9(4)	0.09(4)	-	-
0.9	60	7.46(4)	8.9(2.5)	0.093(27)	-	-
0.95	60	9.45(5)	9.4(1.9)	0.098(20)	7.9(5)	0.083(5)
1.	60	12.04(6)	10.0(1.7)	0.104(18)	8.9(5)	0.093(5)
1.	70		-	-	8.3(5)	0.087(5)
1.05	60	15.42(7)	10.3(1.5)	0.107(16)	10.2(6)	0.106(6)
1.1	60	19.82(9)	11.3(1.5)	0.118(15)	10.5(8)	0.110(8)
1.1	130		-	-	11.1(1.3)	0.115(13)
1.12	60	21.94(10)	10.3(1.4)	0.108(14)	10.9(7)	0.113(7)
1.14	60	24.31(10)	10.7(1.4)	0.111(14)	10.7(7)	0.111(7)
1.16	60	26.93(11)	10.9(1.4)	0.113(14)	10.3(7)	0.107(7)
1.18	60	29.86(12)	10.6(1.4)	0.111(15)	11.4(1.0)	0.118(10)
1.2	60	33.13(13)	10.0(1.3)	0.104(14)	10.5(1.0)	0.110(10)
1.2	180		-	-	13.4(1.5)	0.139(15)

TABLE IX: Comparison of different determinations of $\chi \cdot \xi_G^2 = \chi/M_G^2$: field theoretical method and FP action (column (1), present work), field theoretical method and Symanzik action (column (2), [12]), field theoretical method and CP¹ standard action with explicit gauge degrees of freedom (column (3), [34]), FP charge operator and parametrized FP action¹⁰ (column (4), [13]).

ξ_G	(1)	(2)	(3)	(4)
4.74(3)	0.09(7)	-	-	-
5.92(4)	0.09(4)	-	-	-
6.057(17)	-	-	-	0.1004(9)
7.46(4)	0.093(27)	-	-	-
9.45(5)	0.098(20)	-	-	-
12.04(6)	0.104(18)	-	-	-
12.16(3)	-	-	-	0.1448(15)
15.42(7)	0.107(16)	-	-	-
15.9(9)	-	-	0.11(3)	-
18.56(8)	-	0.117(5)	-	-
19.82(9)	0.118(15)	-	-	-
20.40(9)	-	-	-	0.1893(27)
21.2(1.1)	-	-	0.12(3)	-
21.94(10)	0.108(14)	-	-	-
21.96(9)	-	0.121(7)	-	-
24.31(10)	0.111(14)	-	-	-
24.57(10)	-	0.124(7)	-	-
26.93(11)	0.113(14)	-	-	-
29.10(13)	-	0.126(7)	-	-
29.86(12)	0.111(15)	-	-	-
32.58(13)	-	0.127(8)	-	-
33.13(13)	0.104(14)	-	-	-
34.4(3)	-	-	-	0.224(5)
38.60(16)	-	0.121(10)	-	-

¹⁰We are indebted to M. Blatter and R. Burkhalter for the data relative to Fig. 2 in [13].

FIGURES

FIG. 1. Cooling of small-size 2-instantons with the FP action. Action (dotted line) and topological charge (solid line) of cooled discretized 2-instantons are represented versus their size in lattice units. The cooled configurations have been obtained by performing 100 cooling steps on the discretized instanton solution. The action is reported in units of 4π . The lattice size is 60.

FIG. 2. As in Fig. 1 with the tree level Symanzik improved action.

FIG. 3. Stability under cooling of a small-size 2-instanton. The topological charge of a cooled discretized 2-instanton is represented versus the step of cooling when the FP action (circle), the tree level Symanzik improved action (diamond) and the standard action (triangle) is minimized. The size of the 2-instanton in lattice units is 1.2. The lattice size is 60. The procedure has been repeated 100 times with different random sequences.

FIG. 4. As in Fig. 1 with 1-instantons (constant boundary conditions).

FIG. 5. Transition from $Q_g = 1$ to $Q_g = 0$ during the cooling of a 1-instanton (constant boundary conditions) with the FP action. The behavior of action and topological charge in the geometrical definition is represented versus the cooling step. The instanton size in lattice units is 15, the lattice size is 60.

FIG. 6. Scaling behavior of the lattice topological susceptibility in the geometrical approach χ_g with the FP action. Diamonds represent data from MC simulations; the dotted line is the best fit, corresponding to an exponential decay with $\alpha \simeq 0.83$ (see the text); the solid line is the scaling behavior predicted by the renormalization group. The lattice size is 60.

FIG. 7. Comparison between the perturbative and non-perturbative determination of P – the mixing of χ^L with the unity operator – versus β . The diamonds represent the MC data of χ^L , the circles the outcomes of the heating technique (the solid line is the relative fit); the dotted line is the 4-loop perturbative determination of P , while the dashed line is the best fit of the MC data in the perturbative region ($\beta \geq 1.6$).

FIG. 8. χ/M_G^2 versus ξ_G , the correlation length in lattice units, with the FP action.
 (a) $(\chi^L(\beta) - P(\beta))Z(\beta)^{-2}\xi_G(\beta)^2$ on a 60^2 lattice (diamond);
 (b) χ/M_G^2 extracted by cooling on a 60^2 lattice (square);
 (c) the same quantity of (b) computed on lattices of different sizes keeping $L/\xi_G \sim 6$ (filled square).
 For the sake of legibility, data (b) have been slightly shifted in ξ_G .

Figure 1

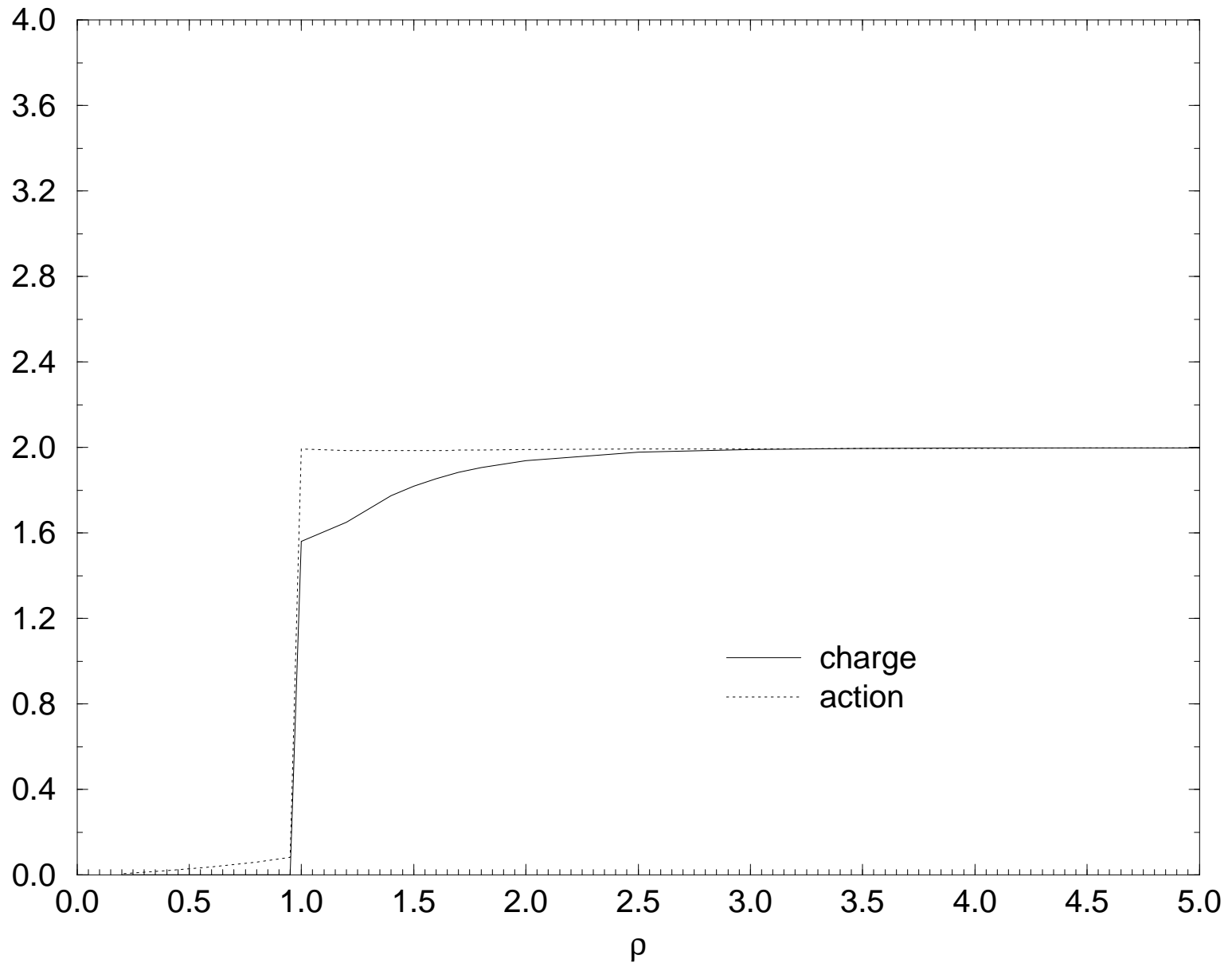


Figure 2

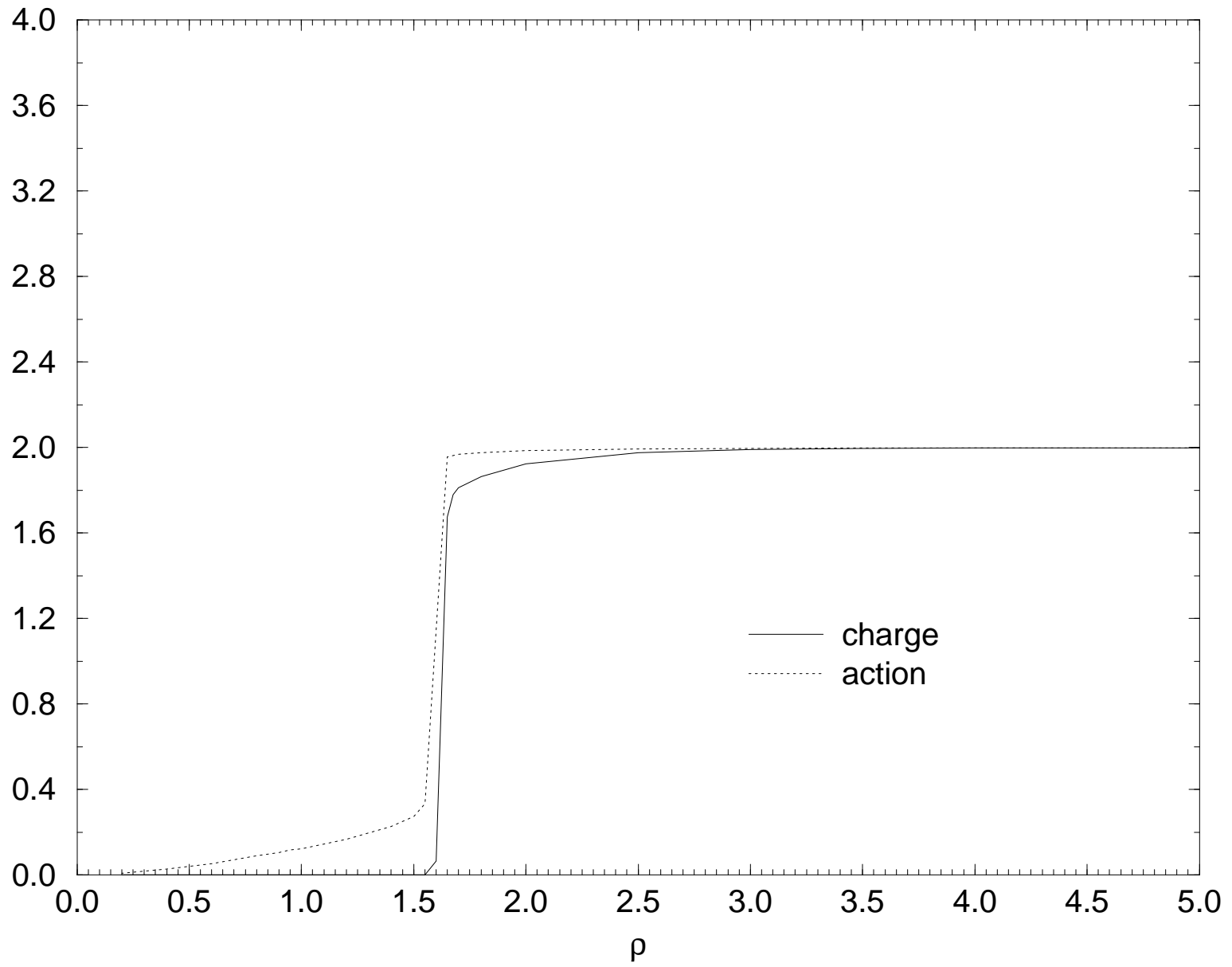


Figure 3

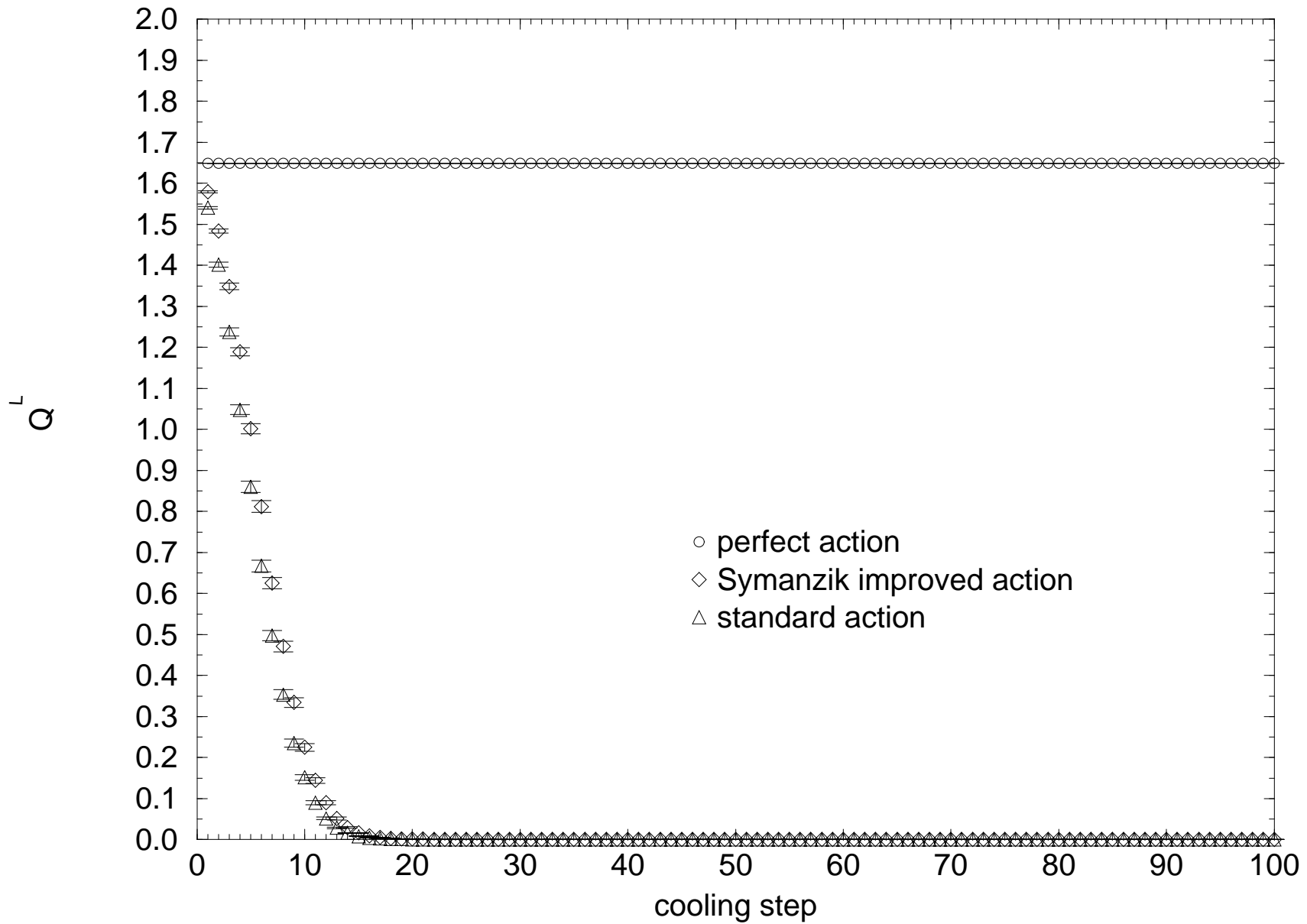


Figure 4

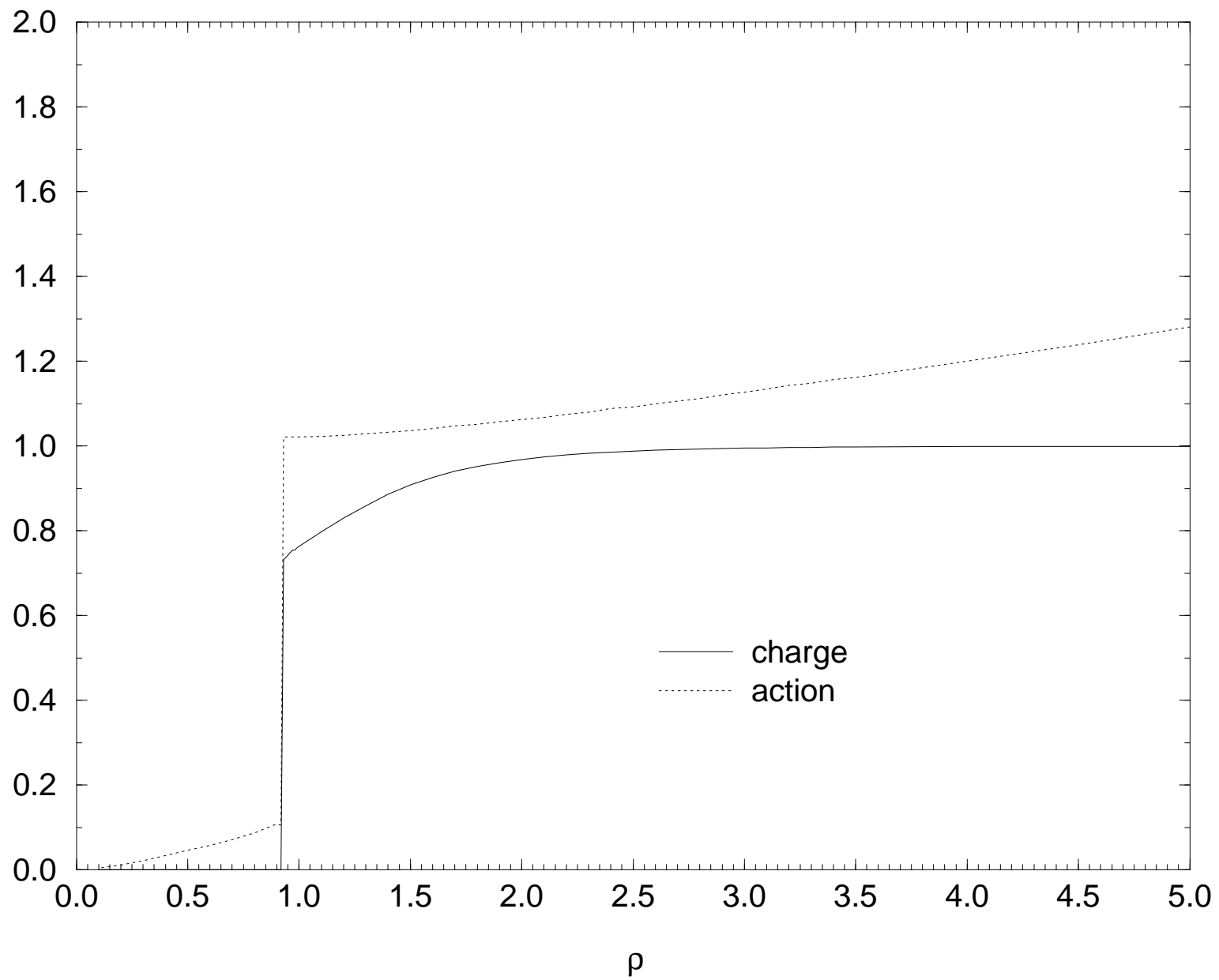


Figure 5

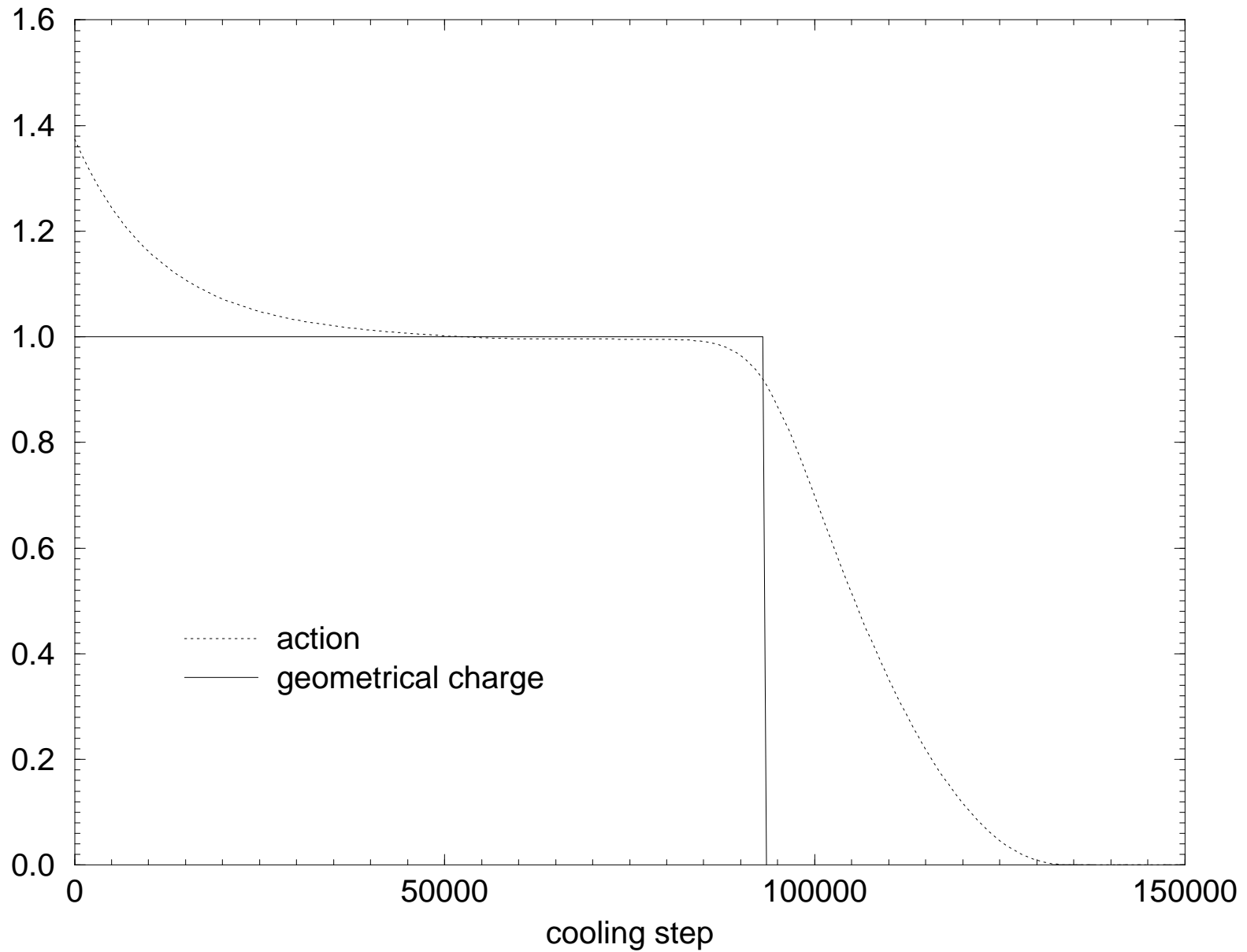


Figure 6

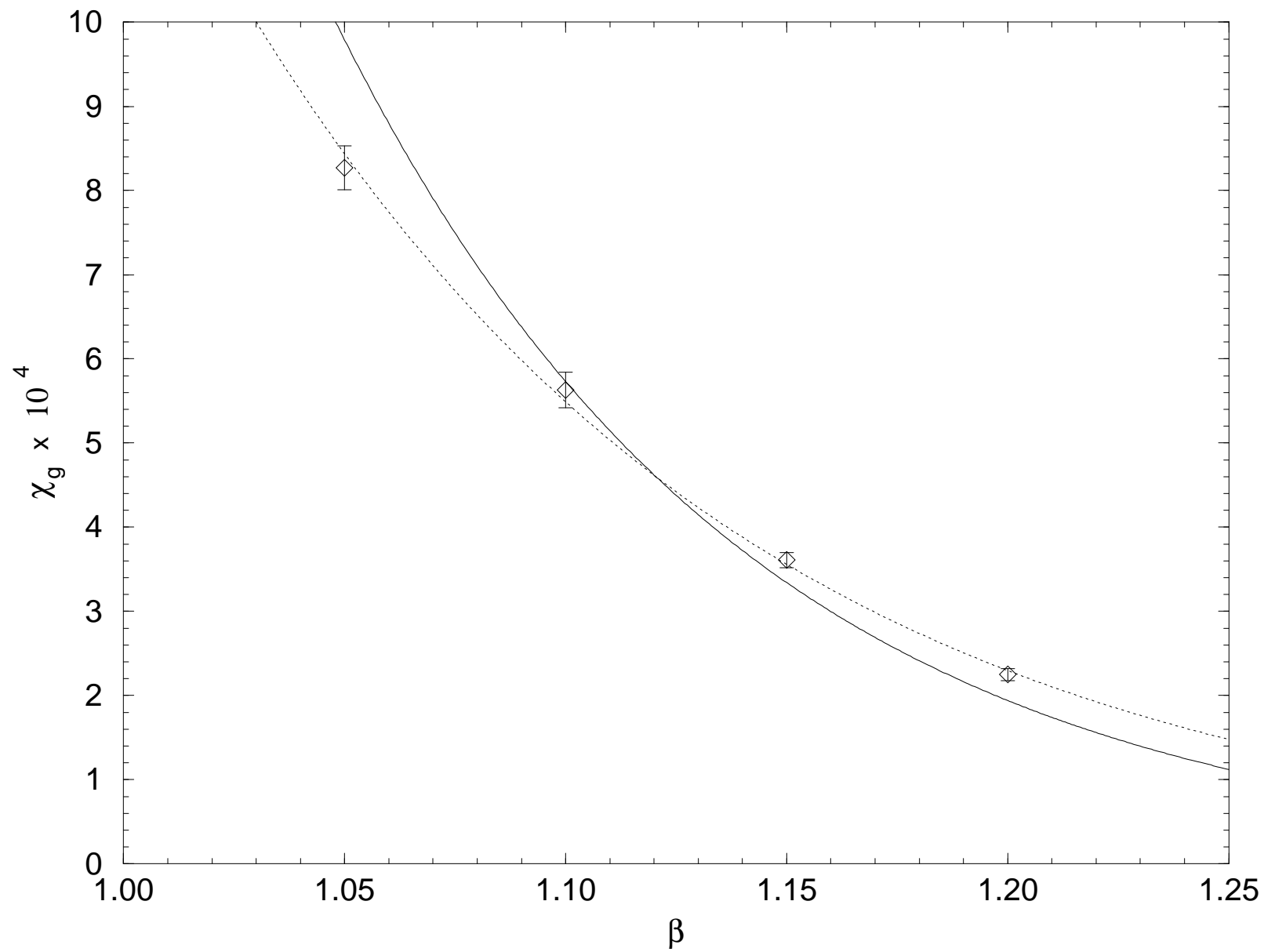


Figure 7

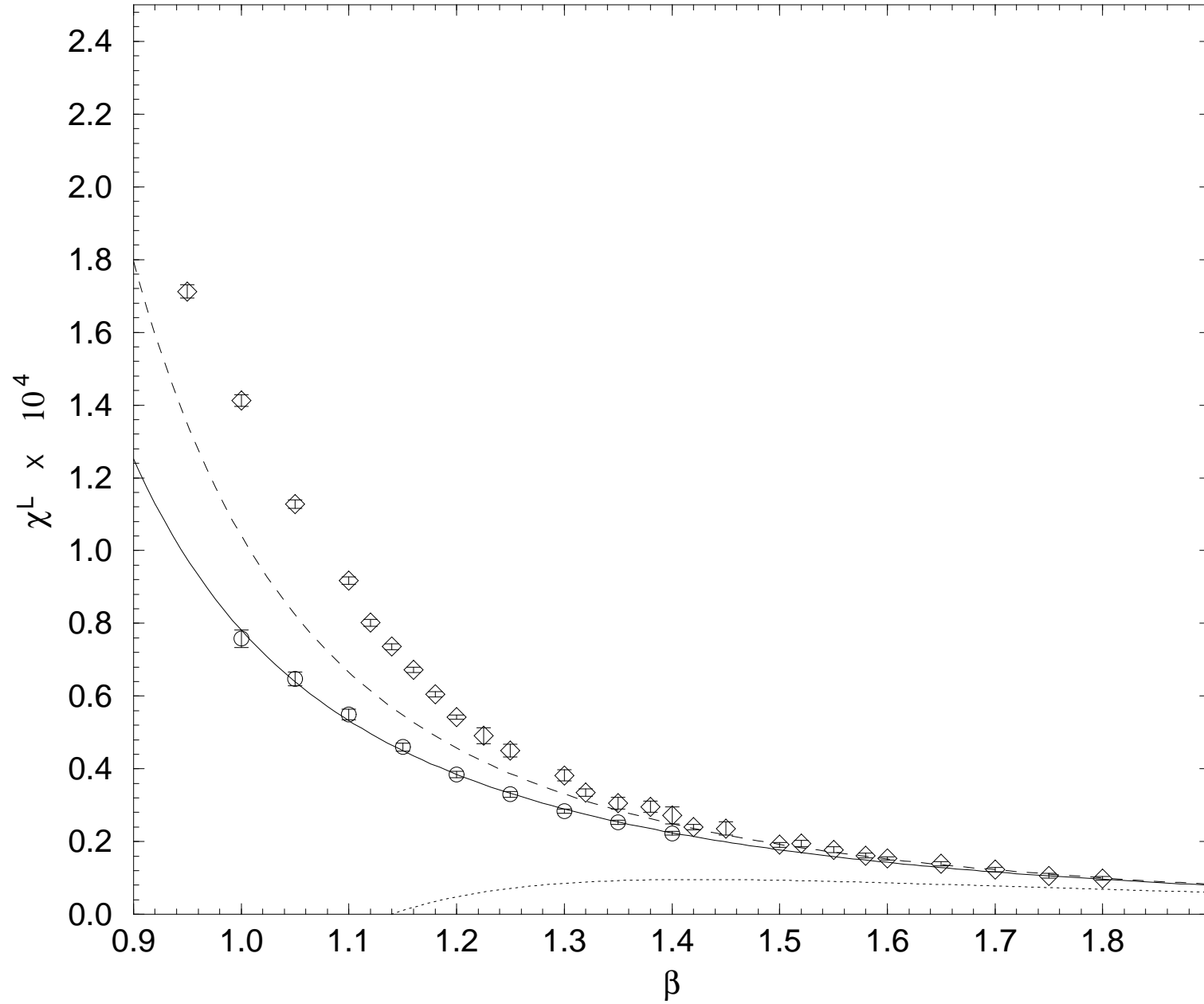


Figure 8

